J-Researchers

Journal of Civil Engineering Researchers

Journal homepage: www.journals-researchers.com

# 2D Equivalent Linear Seismic Site Response Analysis in SBFEM

Morteza Iraniparast, [a] M. Iman Khodakarami [a,*]

[a] *Faculty of Civil Engineering, Semnan university, Semnan, Iran*

**ABSTRACT**

Understanding the dynamic behavior of soil layers under seismic loading is pivotal for accurate seismic design and risk assessment. This study conducts a two-dimensional equivalent linear site response analysis using the Scaled Boundary Finite Element Method with Rayleigh damping to enhanced modeling accuracy. SBFEM combines the advantages of finite and boundary element methods, offering high efficiency in simulating wave propagation and stress concentrations in semi-infinite domains. A MATLAB implementation of the method was validated against previous studies, confirming consistent accuracy across various soil profiles and seismic scenarios. The method demonstrates convergence, accuracy, and stability, requiring fewer elements due to boundary-only discretization. This reduces both computational cost and time while accurately modeling the infinite domain condition. The findings highlight the method's effectiveness for site response analysis under diverse seismic inputs and layered soil configurations, combining the equivalent linear method with SBFEM as a robust and practical tool for dynamic geotechnical applications.

**ARTICLE INFO**

Received: May 21, 2025
Accepted: August 20, 2025

***Keywords:***
*Seismic Site Response Analysis*
*Equivalent Linear*
*Layered Semi-Infinite Soil*
*Scaled Boundary Finite Element Method (SBFEM)*
*Two-dimensional*



DOI: 10.61186/JCER.7.3.52
DOR: 20.1001.1.2538516.2025.7.3.5.5

## 1. Introduction

### *1.1. Site Response Analysis*

Site response analysis is an essential part of geotechnical and earthquake engineering because it evaluates the changes in seismic waves as they propagate through soil and rock layers; therefore, influencing the intensity and traits of ground shaking during earthquakes.

It uses linear, equivalent linear, and non-linear methods for different seismic intensities and soil conditions [1]. Boore [2] discusses the challenges and prospects in predicting site responses, highlighting the complexities and uncertainties in modeling seismic behaviors accurately. Linear methods are used for low-intensity earthquakes and assume elastic soil behavior [3]. In contrast, the equivalent linear method approximates soil's non-linear response for various scenarios [4]. Non-linear methods update soil dynamics at each time step, accurately depicting soil actual stress-strain behavior during high-intensity events [5,6].

For these problems, analytical, semi-analytical, and numerical methods are used in time and frequency domains [7,8].

* Corresponding author. Tel.: +989125314408; e-mail: khodakarami@semnan.ac.ir.

The seismic source, soil complexity, and analysis goals determine the model's dimensionality from 1D to 3D, which affects soil behavior under seismic loads [8-12].

Damping is crucial in site response analysis for capturing energy dissipation mechanisms within soil layers under seismic loads. It significantly reduces seismic energy, affecting both the amplitude and duration of surface ground motion. By incorporating damping into models, predictions of soil behavior during seismic events become more accurate, reflecting the natural energy loss from hysteresis and viscous behavior in soil materials [7,12]. Properly calibrated damping parameters yield more realistic ground motion estimates, particularly vital for high-intensity seismic events [13]. Park and Hashash [14] highlight the importance of precise damping modeling in the context of non-linear time domain site response analysis.

### *1.2. Overview of the Scaled Boundary Finite Element Method for Site Response Analysis*

Introduced by Wolf and Song in 1996 [15], the Scaled Boundary Finite Element Method (SBFEM) evolved from the Consistent Infinitesimal Finite Element Cell Method. SBFEM adeptly handles site response analysis challenges, effectively modeling complex soil profiles and seismic interactions. It adjusts for varying soil properties, dimensions, and boundaries, ensuring precise analysis [16, 17]. SBFEM combines the advantages of Finite Element Method (FEM) and Boundary Element Method (BEM), reducing computational effort by discretizing only domain boundaries, unlike traditional finite element methods [18]. This semi-analytical method accurately captures stress concentrations and wave propagation, ideal for dynamic geotechnical earthquake analysis [16, 17].

Zhang, Wegner, and Haddow [19] utilized SBFEM in a comprehensive three-dimensional dynamic soil-structure interaction analysis in the time domain, providing insights into interactions between soil layers and structures during seismic events. Birk, Prempramote, and Song [20] enhanced SBFEM's utility in time-domain analyses of unbounded domains by introducing an improved high-order transmitting boundary that substantially reduces computational errors from wave reflections at artificial boundaries. Further advancements by Birk, Chen, Song, and Du [21] demonstrated the method's efficacy in transient wave propagation, which broadened its applications in industrial settings. Bazyar and Song [10] developed its applications to transient wave scattering, improving predictions of seismic wave behavior across various soils. Their earlier work, Bazyar and Song [22], expanded its use to non-homogeneous domains, thus enhancing the accuracy of seismic analyses. Additionally, Chen, Birk, and Song [23] extended SBFEM's capabilities to anisotropic soils using a displacement unit-impulse-response-based formulation, pivotal for accurately modeling how anisotropic soil properties affect wave propagation. Yaseri, Bazyar, and Hataf [24] further showcased SBFEM's versatility by applying a 3D coupled scaled boundary finite element/finite element analysis to study ground vibrations induced by underground train movements, demonstrating the method's applicability beyond traditional earthquake engineering contexts.

### *1.3. Equivalent Linear Analysis*

Idriss and Seed [25] first proposed the equivalent linear method for analyzing site response, approximating a non-linear response through a linear analysis of soil layer characteristics during earthquake motions. Subsequently, Schnabel [26], Idriss and Sun [27], and Ordonez [28] implemented the method, adapting it to approximate the nonlinear soil behaviors commonly encountered in earthquake engineering. Various relationships for modulus reduction and damping suitable for equivalent-linear analyses are available, including those by Seed [12], Vucetic and Dobry [29], EPRI [30], Ishibashi and Zhang [31], Darendeli [32], and Zhang, Andrus, and Juang [33].

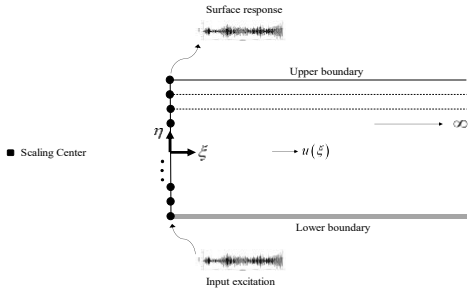


Figure 1. SBFEM applied to semi-infinite layer

In this research, we address the critical challenge of predicting the surface response to earthquake-induced ground motions, which is pivotal for designing resilient structures in seismically active regions. Our approach employs the SBFEM for equivalent linear site response analysis, a sophisticated computational method that models seismic wave propagation in two-dimensional, layered, unbounded domains. This method improves accuracy by incorporating Rayleigh damping and discretizing vertical boundaries with line elements (Fig. 1), effectively simulating real-world seismic conditions. Our research methodology includes a comprehensive comparison of simulated responses—such as acceleration time histories, spectra, and sublayer shear strain and modulus—with actual earthquake data from events like Parkfield and Nahanni. The expected results will underscore the model's precision in capturing complex seismic behaviors and its effectiveness compared to traditional methods, providing

insights into both the strengths and potential limitations of SBFEM in earthquake engineering applications.

## 2. Theoretical Foundations

### *2.1. Formulation of Elastodynamic Equations for Soil Media*

The equation of motion is derived by considering an infinitesimal element of the solid medium:

$$\begin{aligned}\frac{\partial\sigma_x}{\partial x}+\frac{\partial\tau_{xy}}{\partial y}+\frac{\partial\tau_{zx}}{\partial z}+p_x&=\rho\ddot{u}_x\\ \frac{\partial\tau_{xy}}{\partial x}+\frac{\partial\sigma_y}{\partial y}+\frac{\partial\tau_{yz}}{\partial z}+p_y&=\rho\ddot{u}_y\\ \frac{\partial\tau_{zx}}{\partial x}+\frac{\partial\tau_{yz}}{\partial y}+\frac{\partial\sigma_z}{\partial z}+p_z&=\rho\ddot{u}_z\end{aligned} \quad (1)$$

where$\sigma_x$,$\sigma_y$ , and$\sigma_z$ are normal stresses in the $x$,$y$, and $z$ directions; $\tau_{xy}$,$\tau_{zx}$, $\tau_{yz}$, and $\tau_{zx}$ are shear stresses $p_x$,$p_y$, and $p_z$ are the body forces; $\rho$ is the mass density. For $\ddot{u}_x$, $\ddot{u}_y$, and $\ddot{u}_z$, the double dots (¨) indicate the accelerations, i.e. the second time derivatives of displacements. The governing equations for elastodynamics in frequency domain are expressed in Soliman [34].

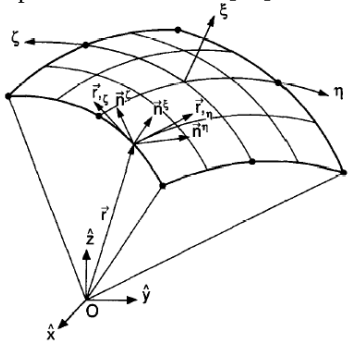


Figure 2. Curvilinear and Cartesian coordinates with surface elements

### *2.2. Coordinate Transformation from Cartesian to Local Systems*

To simplify the governing equations of a medium, the interface is discretized using surface elements, where the points of the elements are related to each other with assumed shape functions. The local coordinates are more suitable, and Cartesian coordinates can translate into these coordinates. Therefore, Curvilinear coordinates are introduced: $\xi$ (radial direction) extends from the origin outward, $\eta$ and $\zeta$(circumferential directions) run parallel to the interface (see Fig. 2 for 2D layered medium). The discretization on the interface, resulting in exact solutions in the radial direction and approximate solutions in the circumferential directions [23, 34].

### *2.3. Discretization Techniques for Motion Equations*

After getting the equation in local coordinate, the governing equation should be solved numerically. To derive a finite-element approximation, the weighted-residual technique is applied to the equilibrium equation [17]. Finally, the SBFEM equation in displacement can be obtained [34].

### *2.4. Derivation of Scaled Boundary Finite Element Equation in time-domain*

After getting the SBFEM equation in displacement, the values of dynamic stiffness need to be obtained too. First of all, internal nodal forces $\{Q(\xi)\}$ should be defined, and for unbounded domain, external nodal force $\{R(\xi)\}$ applied, which is equal to $\{Q(\xi)\}$ with opposite direction. So, the relation between these two forces with respect to the dynamic stiffness $S^{\infty}$($\infty$ stands for infinity) as follows:

$$\{R(\xi)\}=-\{Q(\xi)\}=[S^{\infty}(\omega,\xi)]\{u(\xi)\}-\{R_F(\xi)\} \quad (2)$$

where $\{R_F(\xi)\}$ is the vector of external body forces and boundary traction.

By establishing the relationship between the nodal internal forces and the boundary traction, and employing a weighting function to address approximation errors, the formulation of the dynamic stiffness matrix is derived. Consequently, the SBFEM equation for dynamic stiffness is constructed based on this formulation.

The next step is to express this formulation in the time domain; That process begins by establishing a relationship between two forms of dynamic stiffness: one associated with acceleration response, and the other associated with displacement. After simplification, to transition from the frequency to the time domain, inverse Fourier transformation is applied. Finally, the SBFEM equation in time domain for $\xi=1$ looks like:

$$\begin{aligned}&\int_0^t[m^{\infty}(t-\tau)][m^{\infty}(\tau)]d\tau\\ &\quad+\int_0^t\int_0^{\tau}\left[m^{\infty}(\tau')\right]d\tau'd\tau\left([e_1]^T-\left(\frac{s+1}{2}\right)[I]\right)\\ &+\left([e_1]-\left(\frac{s+1}{2}\right)[I]\right)\int_0^t\int_0^{\tau}\left[m^{\infty}(\tau')\right]d\tau'd\tau\\ &\quad+\frac{t^3}{6}([e_1][e_1]^T-[e_2])\\ &\quad+t\int_0^t[m^{\infty}(\tau)]d\tau-t[m_0]=[0]\end{aligned} \quad (3)$$

where

$$([U]^T)^{-1}[M_0][U]^{-1} = [m_0] \quad (4)$$
$$([U]^T)^{-1}[E_1][U]^{-1} = [e_1]$$
$$([U]^T)^{-1}[E_2][U]^{-1} = [e_2]$$
$$([U]^T)^{-1}[M^{\infty}(t,\xi)][U]^{-1} = [m^{\infty}(t,\xi)]$$

matrices $[E_0(\eta,\zeta)]$, $[E_1(\eta,\zeta)]$ and $[E_2(\eta,\zeta)]$ are the stiffness matrices in a finite element model, and the matrix term $[M_0(\eta,\zeta)]$ is the mass matrix. Decomposing of $[E_0]$ (by using Cholesky decomposition) is:

$$[E_0] = [U]^T[U] \quad (5)$$

where, $[U]$is an upper triangular matrix. Then, inverse matrix of $[E_0]$ is shown below:

$$[E_0]^{-1} = [U]^{-1}[U]^{-T} \quad (6)$$

Also, $[M^{\infty}(\tau,\xi)]$ is the unit impulse response function for acceleration and $[I]$ is the identity matrix. Where the values of $[m_0]$, $[e_1]$ and $[e_2]$ have been given, the only unknown in this equation is the term $[m^{\infty}(t)]$ [22,34 and 35].

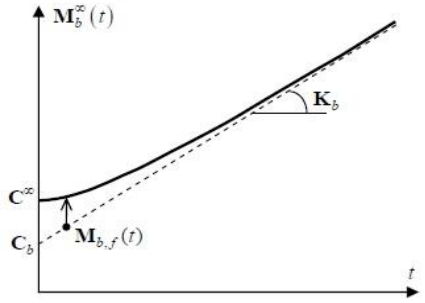


Figure 3. Decomposition of $M_b^{\infty}(t)$

### *2.5. Linear Scheme of Obtaining Acceleration Unit-Impulse Response Matrix*

The integration of Eq. (10) lacks an analytical solution, and thus discretization in time is required for its numerical evaluation. In the original discretization scheme [15, 22], the acceleration unit-impulse response matrix $[M^{\infty}(t)]$is assumed to remain constant within the time step. This method is only conditionally stable and necessitates the use of small-time steps. Furthermore, the computation of integrals involving $[M^{\infty}(t)]$ requires solving a Lyapunov matrix equation at every time step, resulting in a substantial computational burden for large-scale systems.

In the new scheme introduced by Radmanović and Katz [36], a different discretization strategy is adopted wherein the time variation of $[M^{\infty}(t)]$ is modeled as piecewise linear within each time interval. Additionally, the use of an extrapolation parameter $\theta$ enhances the numerical stability of the method, allowing for the use of larger time steps. To further improve computational efficiency, a truncation time is introduced beyond which the $[M^{\infty}(t)]$is assumed to evolve linearly (Fig. 3). This approach leads to a significant reduction in computational cost.

### *2.6. Dynamic Response Calculation of Soil Systems*

The equation of motion of the soil in the time domain can be written as:

$$[M]\{\ddot{u}(t)\} + [C]\{\dot{u}(t)\} + [K]\{u(t)\} = \{P(t)\} - \{R(t)\} \quad (7)$$

where $[M]$, $[C]$ and $[K]$ represent the mass, damping and stiffness matrices of the soil, $\{\ddot{u}(t)\}$, $\{\dot{u}(t)\}$ and $\{u(t)\}$for acceleration, velocity and displacement respectively, while $\{P(t)\}$ and $\{R(t)\}$ are the applied force and the reaction of the unbounded domain, respectively.

In the SBFEM, the mass matrix is derived from the physical properties of the system's elements, including density and geometric configuration. The stiffness matrix characterizes the system's resistance to deformation and is computed based on material properties such as Young's modulus and Poisson's ratio, along with the geometric arrangement of the elements [16].

The calculation of the Rayleigh damping matrix involves a systematic approach, starting from the computation of eigenvalues and natural frequencies to the final construction of the damping matrix. This method ensures that the dynamic behavior of the system is accurately characterized. The first step is to determine the eigenvalues of the system, which are essential in understanding the dynamic characteristics. Eigenvalues are computed through an eigenvalue analysis of the system matrices, specifically the mass and stiffness matrices. This problem is expressed as:

$$[K]v = \lambda[M]v \quad (8)$$

where $\lambda$ represents the eigenvalues, and $v$ are the corresponding eigenvectors. The eigenvalues are then used to calculate the natural frequencies $\omega$ by taking the square root:

$$\omega = \sqrt{\lambda} \quad (9)$$

Natural frequencies are crucial as they represent the inherent vibrational properties of the system. Once the natural frequencies are obtained, the next step is to determine the Rayleigh damping coefficients, $\alpha$ and $\beta$. Rayleigh damping is a proportional damping model where the damping matrix $[C]$ is a linear combination of the mass and stiffness matrices. The coefficients are derived to achieve a specified damping ratio $\xi_D$ at two selected frequencies. The system of equations for $\alpha$ and $\beta$ is formulated as:

$$\begin{bmatrix} 1 & \omega_1^2 \\ 1 & \omega_2^2 \end{bmatrix} \begin{bmatrix} \alpha \\ \beta \end{bmatrix} = \begin{bmatrix} 2\xi_D \\ 2\xi_D \end{bmatrix} \quad (10)$$

Here, $\omega_1$ and $\omega_2$ are the chosen natural frequencies. Solving this system yields the values for $\alpha$ and $\beta$, and with these determined coefficients, the damping matrix $[C]$ can be constructed. The damping matrix is expressed as:

$$[C] = \alpha[M] + \beta[K] \quad (11)$$

This linear combination ensures that the damping characteristics are appropriately distributed within the system, corresponding to the specified damping ratio at the selected frequencies [15, 37].

The interacting force-acceleration relationship for the soil in the time domain can be represented by the convolution integral as [36]:

$$\{R(t)\} = \int [M^{\infty}(\tau)]\{\ddot{u}(t-\tau)\}d\tau \quad (12)$$

In the detailed analysis of seismic response within soil layers, accurately computing the shear strain is crucial for assessing the structural integrity and dynamic behavior of the soil under seismic forces. This process begins with the acquisition of nodal displacements, which are essentially the movement of predefined points within the soil matrix during seismic activity. Each node's displacement is recorded in a two-dimensional space, allowing for the subsequent computation of displacement gradients.

The displacement gradient is a fundamental concept in continuum mechanics, representing the rate of change of displacement across a finite distance within the material. In this analysis, the displacement gradient is mathematically defined by the difference in displacements between adjacent nodes, normalized by the spatial distance between these nodes. This calculation provides a local view of deformation specific to the area around each node.

Following the determination of displacement gradients, the deformation gradient tensor, $H$, is calculated. This tensor is pivotal in transitioning from the undeformed state to the deformed state of the soil element, encapsulating both rotational and translational deformation components. The tensor is computed as:

$$H = I + \nabla u \quad (13)$$

where $I$ represents the identity matrix and $\nabla u$ is the displacement gradient tensor [38]. Subsequently, the Green-Lagrange strain tensor,$E$, is derived to measure the strain experienced by the soil element relative to its original configuration. The tensor is calculated using as:

$$E = \frac{1}{2}(H^T H - I) \quad (14)$$

where $H^T$ is the transpose of the deformation gradient tensor. This expression captures the quadratic contributions of the deformation, essential for describing strains in scenarios involving displacements and rotations typical in seismic activities. The final step involves extracting the engineering shear strain,$\gamma$, from the Green-Lagrange strain tensor. The shear strain, specifically, is calculated as twice the value of the off-diagonal component of the tensor $S$, that is (assuming symmetry $E_{12} = E_{21}$):

$$\gamma = 2E_{12} \quad (15)$$

This value, engineering shear strain, is crucial because it quantifies the material's deformation under shear loading, thereby reflecting its capacity to withstand seismic-induced stresses.

### *2.7. Equivalent Linear Approach*

The linear model is the foundational constitutive model for site response, treating soil behavior as viscoelastic. It assumes a constant equivalent viscous damping ratio, unaffected by strain level or frequency. Using the small-strain shear modulus $G_{s\,max}^2$, derived from the soil's shear-wave velocity ($V_s$) and density ($\rho$), this model enables linear site-response analysis with inputs like shear-wave velocity, density, damping ratio, and base motion.

Unlike linear models with fixed soil properties, the equivalent linear method approximates nonlinear soil behavior by adjusting properties based on strain levels from cyclic loading. It divides the soil into sub-layers, improving seismic response predictions and enabling detailed analysis of interlayer interactions. This method offers a practical balance between computational efficiency and accuracy, especially when full nonlinear analysis is impractical.

In addition to the parameters used in linear models, the equivalent-linear approach requires strain-dependent modulus-reduction and damping curves. Shear modulus and damping are iteratively adjusted to match the effective shear strain and then held constant during each loading cycle. This tuning, based on peak strain, improves predictions of peak strains and displacements. In this study, we used Seed's [12] relationships for modulus-reduction and damping, modeling stress-strain behavior in layers above the bedrock. Calculations used a strain ratio of 0.65, with up to 20 iterations, and sublayers no thicker than 1 meter. After each iteration, shear modulus and damping were evaluated and compared with previous values for all sublayers to ensure convergence.

Fig. 4 presents a flowchart outlining the equivalent linear site response analysis using the SBFEM. It summarizes key steps from problem setup, material property input, and element selection to dynamic response calculation. This structured approach emphasizes accurate soil behavior modeling under seismic loading. The algorithm accommodates 2D, 3D, or axisymmetric problems, with inputs as force, displacement, or acceleration (this study considers a 2D in-plane acceleration case under sinusoidal and earthquake loading). Essential soil properties—Poisson's ratio, density, and shear wave velocity—are used to assign materials. Depending on the problem, elements such as L2 and L3 (2D) or Q4, Q8, Q9 (3D) are selected [39]. This analysis uses two-node elements with two degrees of freedom each. Once materials and elements are defined, soil layering is performed. Node coordinates are assigned counterclockwise around the scaling center, and boundary restraints and matrix dimensions are set. The total analysis time is defined by excitation duration and the time step, including that for unit impulse response. Subdividing soil

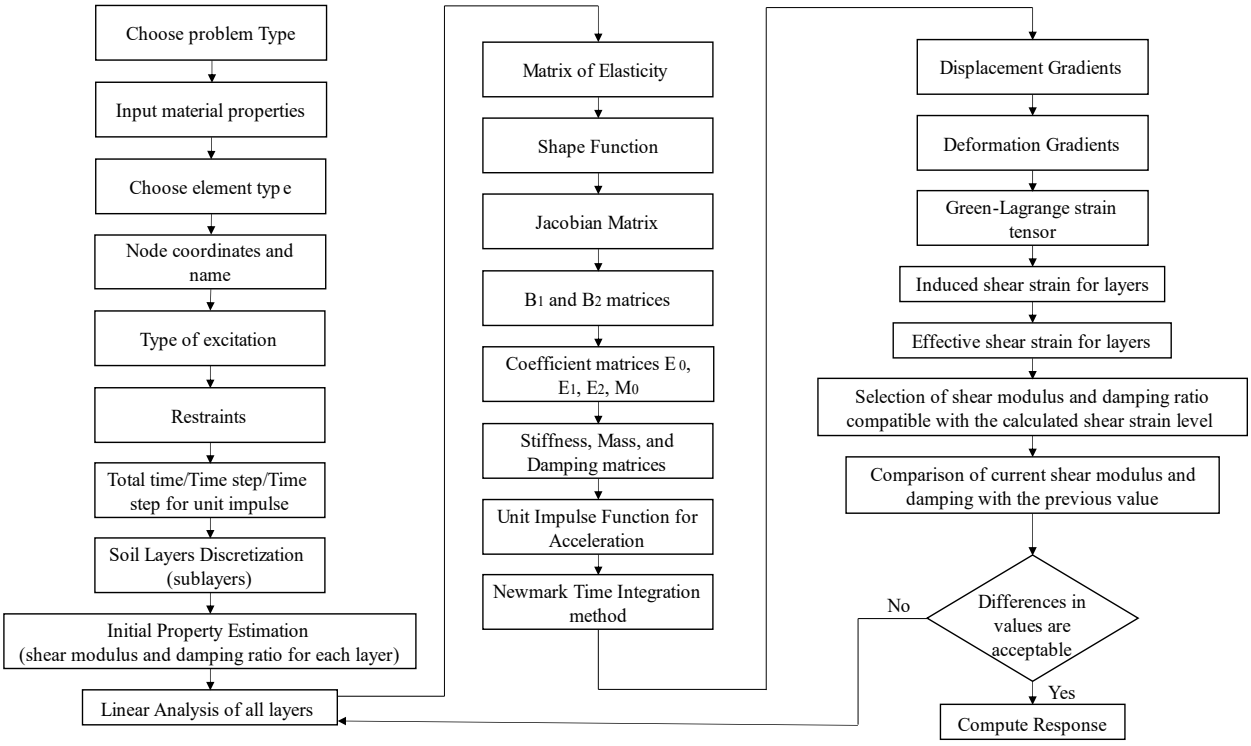


Figure 4. Flowchart of Equivalent Linear approach for layered soil

Table 1.
Characteristics of Earthquakes

| Earthquake | Date | Location | Peak Ground Acceleration (PGA) | Peak Ground Velocity (PGV) | Vmax/Amax |
|---|---|---|---|---|---|
| Parkfield | September 28, 2004 | Near Parkfield, California | 0.35736 g | 21.48479 cm/s | 0.06129 sec |
| Nahanni | December 23, 1985 | Nahanni Region, Northwest Territories, Canada | 0.14275 g | 6.06058 cm/s | 0.04328 sec |

Table 2.
Soil layers properties

| Shear Wave Velocity m/s | Density kg/m³ | Unit Weight kN/m³ | Poisson's ratio |
|---|---|---|---|
| 200 | 1836 | 18 | 0.4 |
| 300 | 1938 | 19 | 0.35 |
| 500 | 2040 | 20 | 0.3 |
| 700 (Bedrock) | - | 22 | - |

layers into thinner sublayers enhances accuracy. The analysis begins with initial shear modulus and damping values at low strain. These are updated iteratively based on effective strain using empirical relationships. If differences between iterations fall within an acceptable range, the results are finalized; otherwise, the process continues until convergence or the iteration limit is reached.

This methodology is particularly effective in stratigraphically complex conditions, where varying mechanical properties across layers significantly affect seismic response. Iterative updates to modulus and damping are essential for accurately predicting ground motion. By analyzing each layer in relation to adjacent ones, the method offers a clear understanding of seismic wave amplification and energy dissipation throughout the soil profile.

## 3. Verification

### *3.1. Selection of Input Motions and Description of Soil Profiles*

#### *3.1.1. Overview of Seismic Input and Soil Configurations*

To rigorously compare the outputs from the proposed approach with those from DEEPSOIL and QUAKE/W, a variety of input motions were used. These included sinusoidal excitations and actual earthquake such as the Parkfield and Nahanni earthquakes, categorized as in-plane motions.

Table 1 provides detailed specifications of the seismic events used in the verification studies, namely the Parkfield

and Nahanni earthquakes. Additionally, the properties of the soil layers in the analyzed profiles are summarized in the Table 2.

### *3.1.2. Sinusoidal Excitations and Soil Profiles*

This section details the setup for simulations using sinusoidal excitations on various soil profiles. Each profile is designed to understand the response of different soil types under controlled vibratory conditions.

- Soil Profiles: Three single-layer soil profiles are considered, see Table 3 and Fig. 5.
- Excitation Characteristics: The excitations are applied for a duration of 10 seconds and feature a periodicity of 0.4 seconds. The amplitude of the sinusoidal waves varies, with tests conducted at 0.375g, 0.75g, 1.5g, and 3g (respectively excitations SI, SII, SIII and SIV), see Fig. 6.

Table 3.
Soil profiles for sinusoidal excitations

| Profile | No. of Layers | Layer Thickness (m) | Shear Wave Velocity (m/s) |
|---|---|---|---|
| S500 | 1 | 30 | 500 |
| S300 | 1 | 30 | 300 |
| S200 | 1 | 30 | 200 |

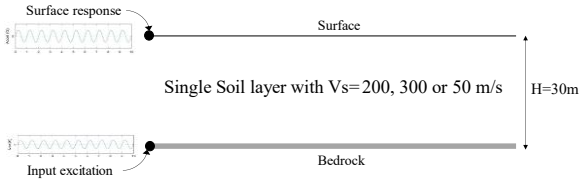


Figure 5. Soil profile with single layer

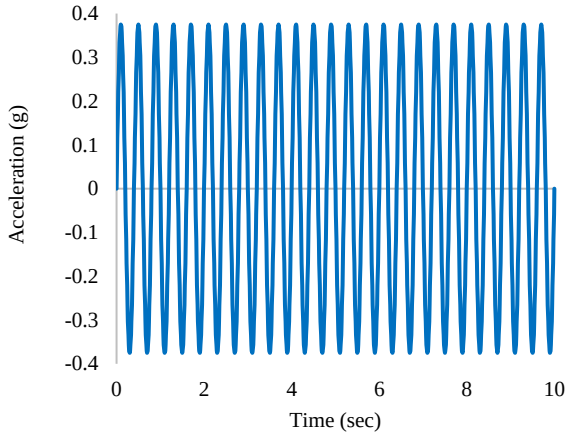


Figure 6. Input motion with amplitude of 0.375g

### *3.1.3. Parkfield Earthquakes and Soil Profiles*

- Soil Profiles: The details of the six soil profiles under the Parkfield earthquake are shown in Table 4 and Fig. 7.
- Duration and Intensity: The duration of the earthquake simulation is 10 seconds, with intensity levels adjusted to half, original, and double the original recorded scales (respectively excitations EI, EII, EIII), see Fig. 8.

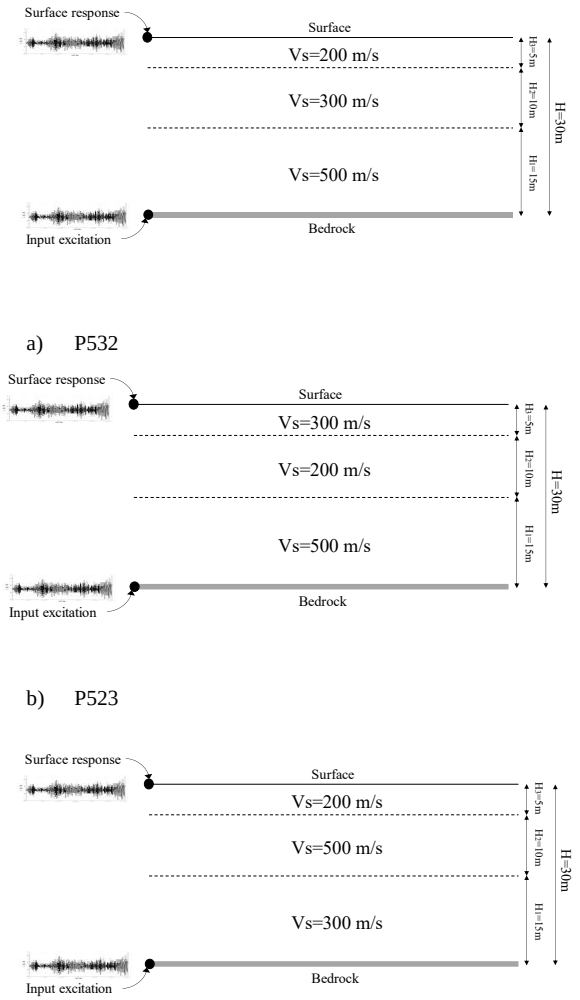


Figure 7. Three-layer soil profiles

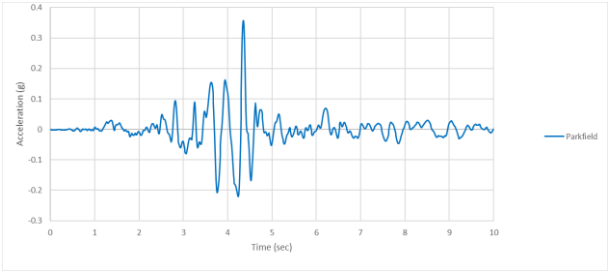


Figure 8. Original Parkfield earthquake

*3.1.4. Nahanni Earthquakes and Soil Profiles*

- Soil Profiles: Further validation is performed using data from the Nahanni earthquake, applying similar profiles as those in the Parkfield scenarios but adjusting for the unique characteristics of the Nahanni event and the prefix N instead of P is used in naming the profiles (such as N500, N300, etc.).
- Duration and Intensity: The duration for these tests extends to 19 seconds to accommodate the longer-lasting Nahanni earthquake dynamics, with intensity variations also set at half, original, and double the original scale (respectively excitations QI, QII, QIII), see Fig. 9.

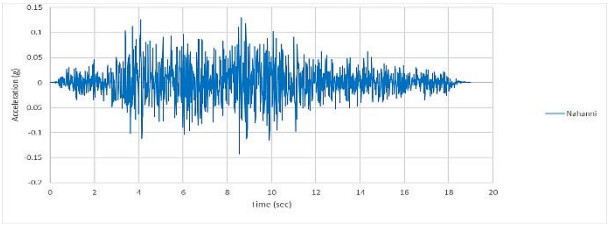


Figure 9. Original Nahanni earthquake

This section aims to not only verify the accuracy of the proposed approach but also to highlight the comparative efficiency and applicability of the proposed approach, DEEPSOIL, and QUAKE/W in handling diverse seismic scenarios.

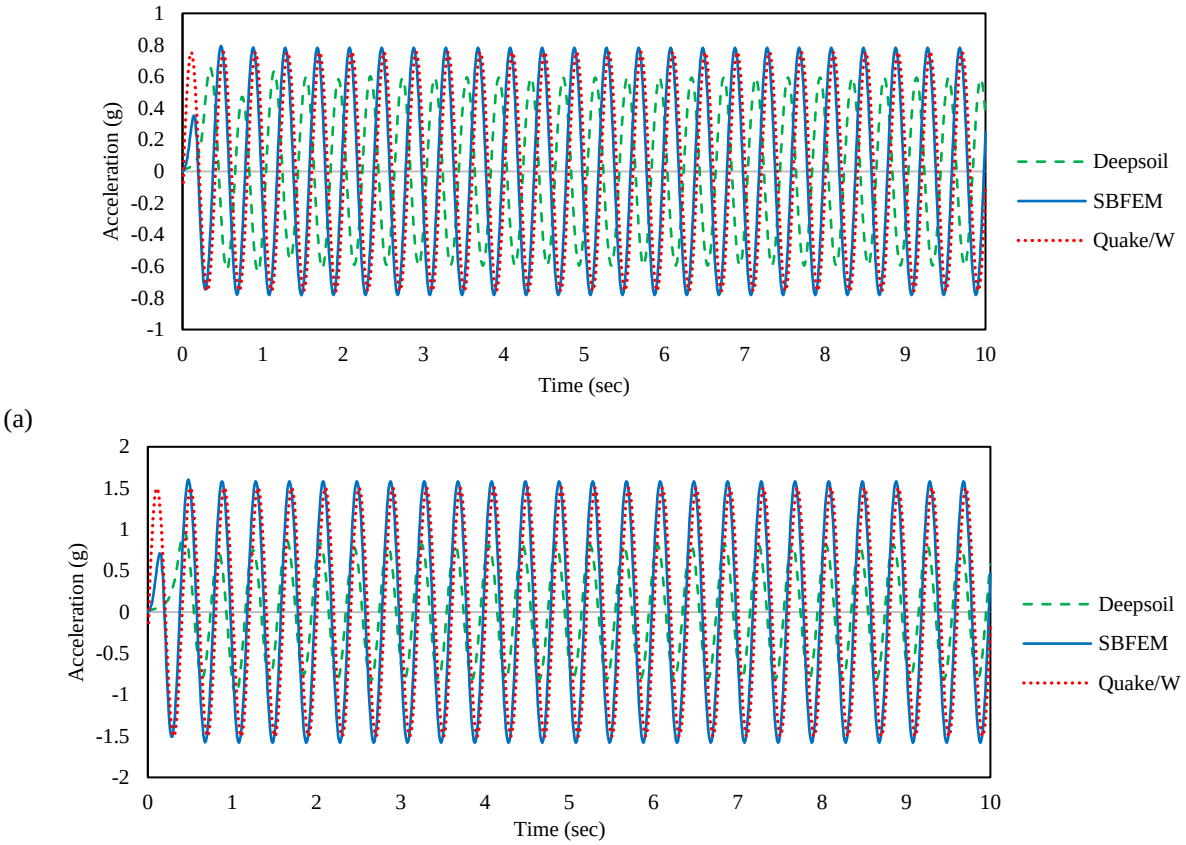


Figure 10. Response acceleration time history of profile S300 for sinusoidal excitations of a) A=0.75g and b) A=1.5g

## 4. Comparative Analysis of Site Response Under Various Seismic Conditions

*4.1. Analysis Results from Sinusoidal Excitations*

The results from the sinusoidal excitation tests offer a comprehensive analysis of how single-layer soil profiles respond to varying seismic load amplitudes, utilizing the SBFEM as implemented in MATLAB. The acceleration time histories recorded at the surface are juxtaposed with results from established geotechnical analysis software, namely DEEPSOIL and QUAKE/W, to validate the proposed approach's efficacy.

Fig. 10, as the sample, illustrates the surface acceleration time history for a single-layer soil profile with a shear wave velocity of 300 m $s^{-1}$ (S300) under excitations

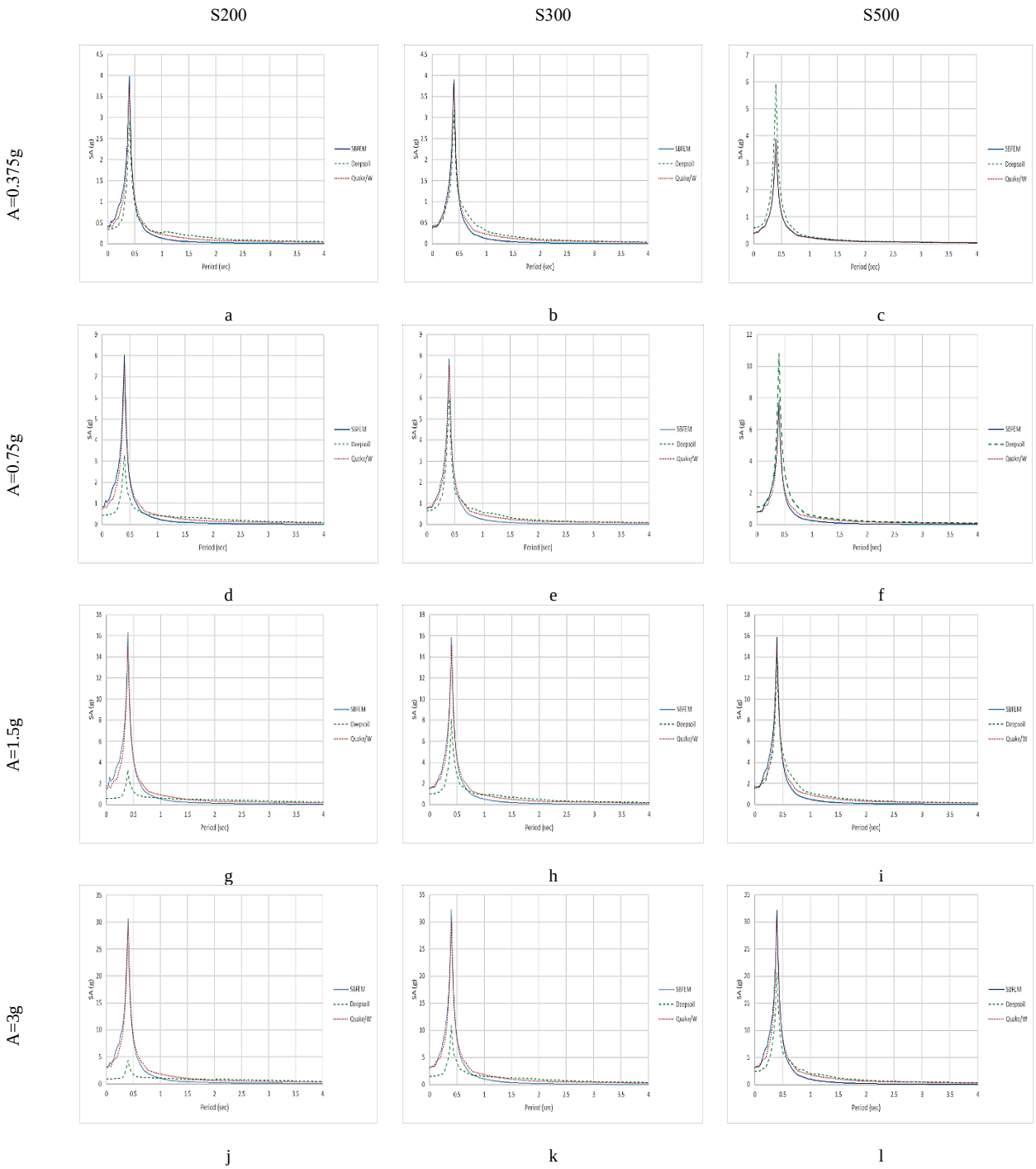


Figure 11. Acceleration response spectrum of sinusoidal excitations of single layer soils

SII and SIII. The response acceleration time histories for single-layer soil profiles (S200, S300, S500) under sinusoidal excitation show that the SBFEM closely matches QUAKE/W results, particularly at higher shear wave velocities. For instance, in the S200 profile under excitation SI, peak accelerations from SBFEM and QUAKE/W differed by only 8%, while DEEPSOIL deviated by 25% with a 0.1-second phase shift. In stiffer soils like S500, DEEPSOIL discrepancies increased to 33% in peak acceleration and 0.15 seconds in timing. Under excitation SIII, SBFEM demonstrated reliable performance in the S500 profile, with peak acceleration differences of respectively 12% and 4% compared to DEEPSOIL and QUAKE/W.

Fig. 11 presents the surface acceleration response spectrum under sinusoidal excitations. For example, Fig.

Table 5.
The peak percentage difference in the acceleration response spectrum of SBFEM compared to DEEPSOIL and QUAKE/W for sinusoidal excitation

| | | Profile | | | | | |
|---|---|---|---|---|---|---|---|
| | | S200 | | S300 | | S500 | |
| | | DEEPSOIL | QUAKE/W | DEEPSOIL | QUAKE/W | DEEPSOIL | QUAKE/W |
| Excitation | SI | -35.1 | -6.1 | -22.7 | -2.5 | 34.6 | 0.0 |
| | SII | -145.3 | -7.2 | -31.5 | -3.7 | 27.1 | -3.0 |
| | SIII | -396.9 | -9.1 | -94.5 | -5.2 | -13.6 | -4.5 |
| | SIV | -595.8 | -2.3 | -195.3 | -7.2 | -56.1 | -6.3 |

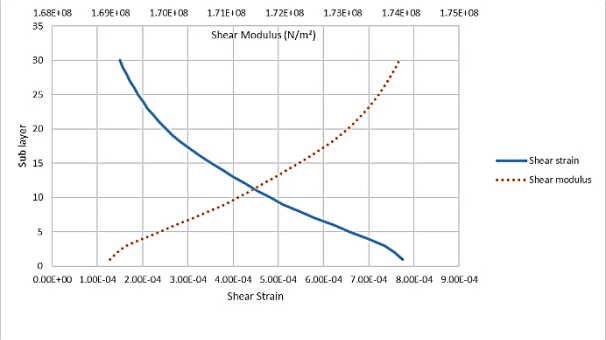


Figure 12. Shear strain and shear modulus of sublayers of profile S300 for sinusoidal excitation amplitudes A=0.75g

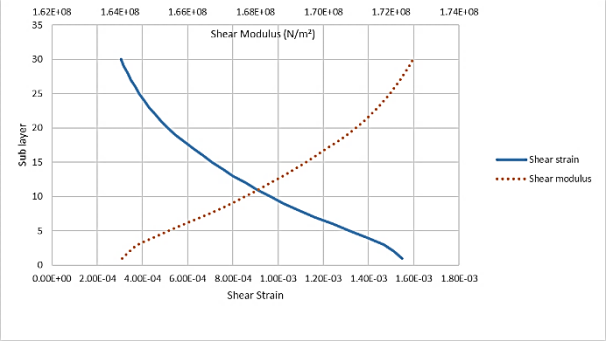


Figure 13. Shear strain and shear modulus of sublayers of profile S300 for sinusoidal excitation amplitudes A=1.5g

11a shows a peak at the soil's natural frequency, indicating resonance, with SBFEM and QUAKE/W closely matching, while DEEPSOIL shows slight deviations. Table 5 shows the percentage differences in peak spectral values between SBFEM and both DEEPSOIL and QUAKE/W, with signs indicating whether the reference method over- or underestimates the SBFEM result. The response spectra from Fig. 11a to Fig. 11l show consistent agreement between SBFEM and QUAKE/W, especially at primary resonance frequencies and peak accelerations, confirming both methods' ability to capture key dynamic behavior. At higher frequencies, DEEPSOIL aligns more closely with QUAKE/W than with SBFEM.

Fig. 12 and Fig. 13, serving as examples, illustrate the mechanical behavior of the S300 soil profile under A=0.75g and A=1.5g sinusoidal excitations, showing shear strain and shear modulus variations across the vertical profile. These figures provide key insights into deformation mechanisms and soil stiffness changes during seismic loading. All soil profiles show that shear strain is highest in the deepest layers near the excitation source and decreases toward the surface as wave energy dissipates. The S500 profile under excitation SI exhibits lower shear strains at all depths than S200 and S300, due to its higher stiffness affecting strain distribution. Across all soil profiles, shear modulus increases from the deepest layers to the surface, reflecting typical seismic soil behavior where higher strains cause soil softening. This trend highlights how seismic energy absorption reduces stiffness in deeper layers under higher strain conditions.

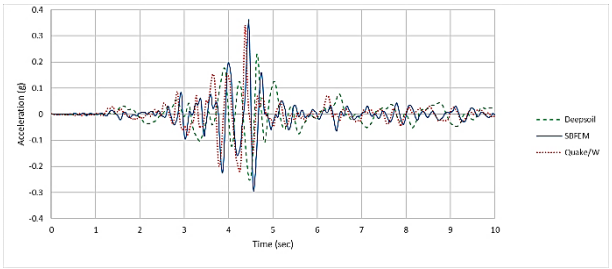


Figure 14. Response acceleration time history of profile P200 for excitation EII of Parkfield earthquake

### *4.2. Response Analysis of Parkfield Earthquake Simulations*

The Parkfield earthquake analysis on single-layer soil profiles (P200, P300, P500) offers insights into dynamic responses under different seismic intensities. Three intensity levels (EI, EII, EIII) were used to assess soil behavior under varying stress conditions.

Fig. 14, as the sample, shows the surface acceleration time history for the P200 profile under excitation EII using SBFEM, compared against DEEPSOIL and QUAKE/W results. Under excitation EI, SBFEM slightly overestimates P200 by 6%, consistent with QUAKE/W and DEEPSOIL. For P300 and P500 under the same excitation, DEEPSOIL records peak accelerations 26% and 31% higher than SBFEM. In excitation EII, SBFEM yields higher accelerations for P200, exceeding DEEPSOIL and

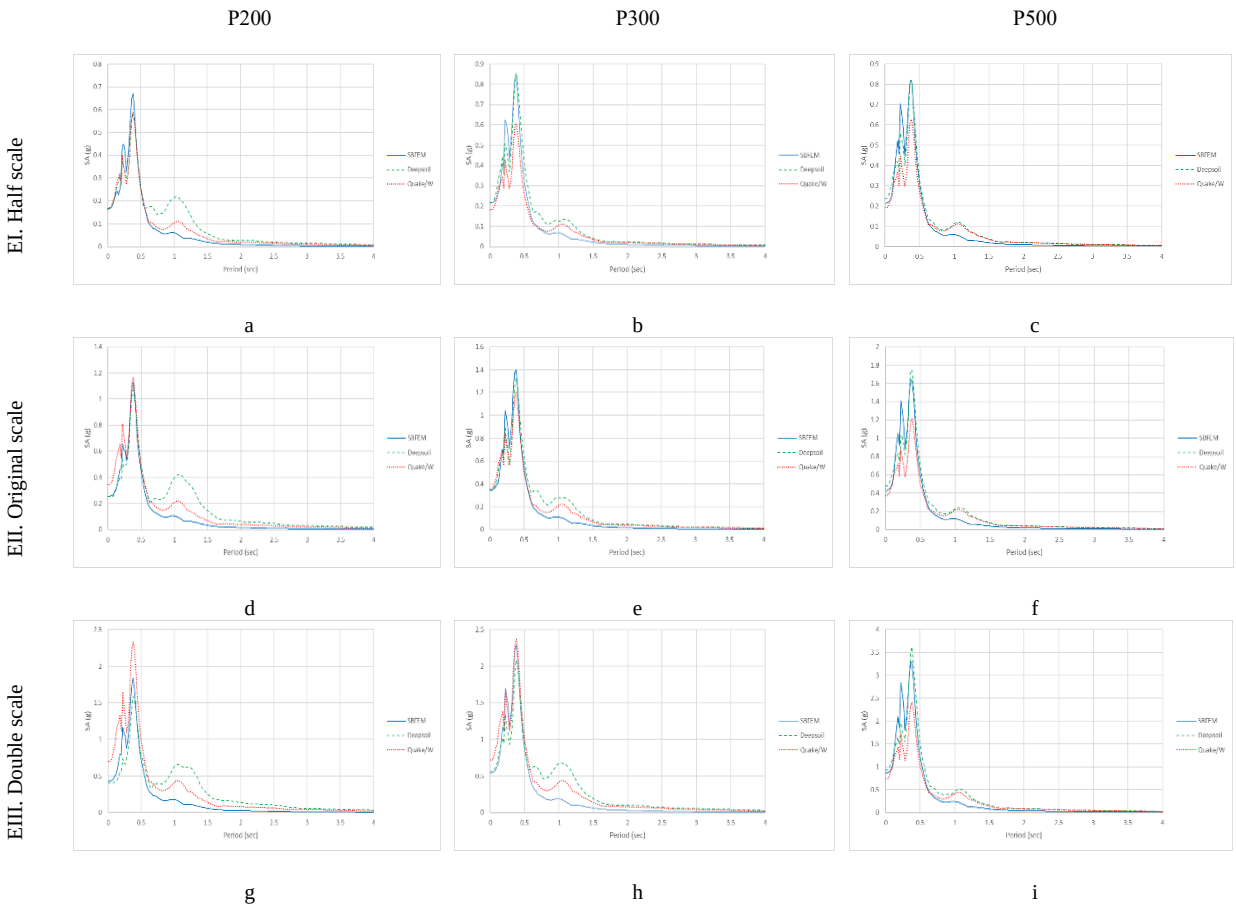


Figure 15. Acceleration response spectrum of Parkfield earthquakes for single layer soils

Table 6.
The peak percentage difference in the acceleration response spectrum of SBFEM compared to DEEPSOIL and QUAKE/W for Parkfield excitations of single layer profile

| | | Profile | | | | | |
|---|---|---|---|---|---|---|---|
| | | P200 | | P300 | | P500 | |
| | | DEEPSOIL | QUAKE/W | DEEPSOIL | QUAKE/W | DEEPSOIL | QUAKE/W |
| Excitation | EI | -13.2 | -14.4 | 0.6 | -39.8 | 0.6 | -30.1 |
| | EII | -5.3 | 3.6 | -5.8 | -16.9 | 6.5 | -34.0 |
| | EIII | -15.7 | 21.3 | -9.8 | 3.3 | 9.2 | -36.8 |

QUAKE/W by 4% and 42%, respectively, with smaller differences in stiffer profiles (P300 and P500). Under excitation EIII, larger discrepancies occur for P200, where QUAKE/W exceeds SBFEM by over 48%, while differences in P300 and P500 are less pronounced.

Fig. 15 presents the surface acceleration response spectra for each soil profile and earthquake intensity, illustrating the soil layers' frequency response. Table 6 lists the percentage differences in peak spectral values compared to DEEPSOIL and QUAKE/W. In Fig. 15a, SBFEM predicts higher spectral accelerations at the predominant period, while QUAKE/W and DEEPSOIL align closely. In Fig. 15b and Fig. 15c, SBFEM matches DEEPSOIL at low periods, and DEEPSOIL matches QUAKE/W at mid to high periods. All methods show consistent phase responses, but amplitude differences reflect variations in energy distribution modeling. Fig. 15g, Fig. 15h, and Fig. 15i extend these spectral trends.

Fig. 16, a representative case, illustrates the final shear strain and shear modulus distribution for the P200 profile under excitation EII, highlighting variations in strain magnitude and soil stiffness across the sublayers. All profiles show lower shear strain at depth, reflecting the intrinsic characteristics of soil layers. Shear modulus consistently increases toward the surface, independent of seismic scaling, indicating mechanical stiffening with

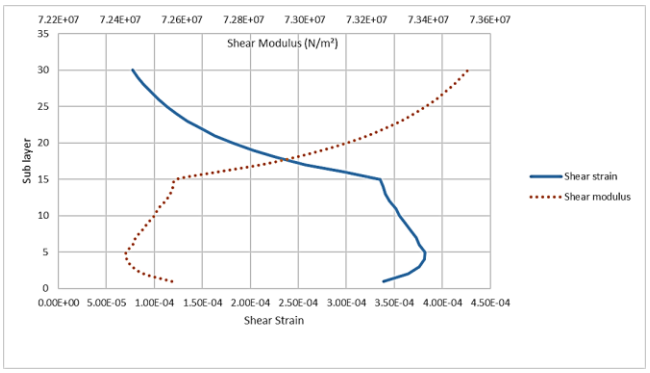


Figure 16. Shear strain and shear modulus of sublayers of profile P200 for excitation EII of Parkfield earthquake

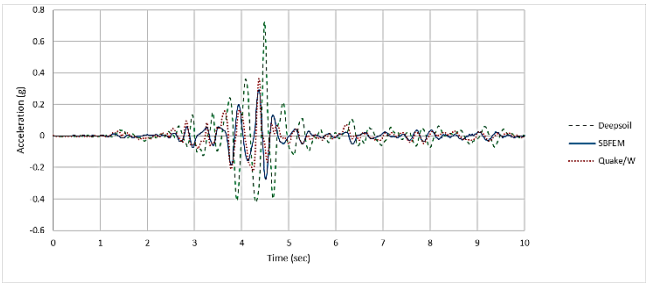


Figure 17. Response acceleration time history of profile P532 for excitation EII of Parkfield earthquake

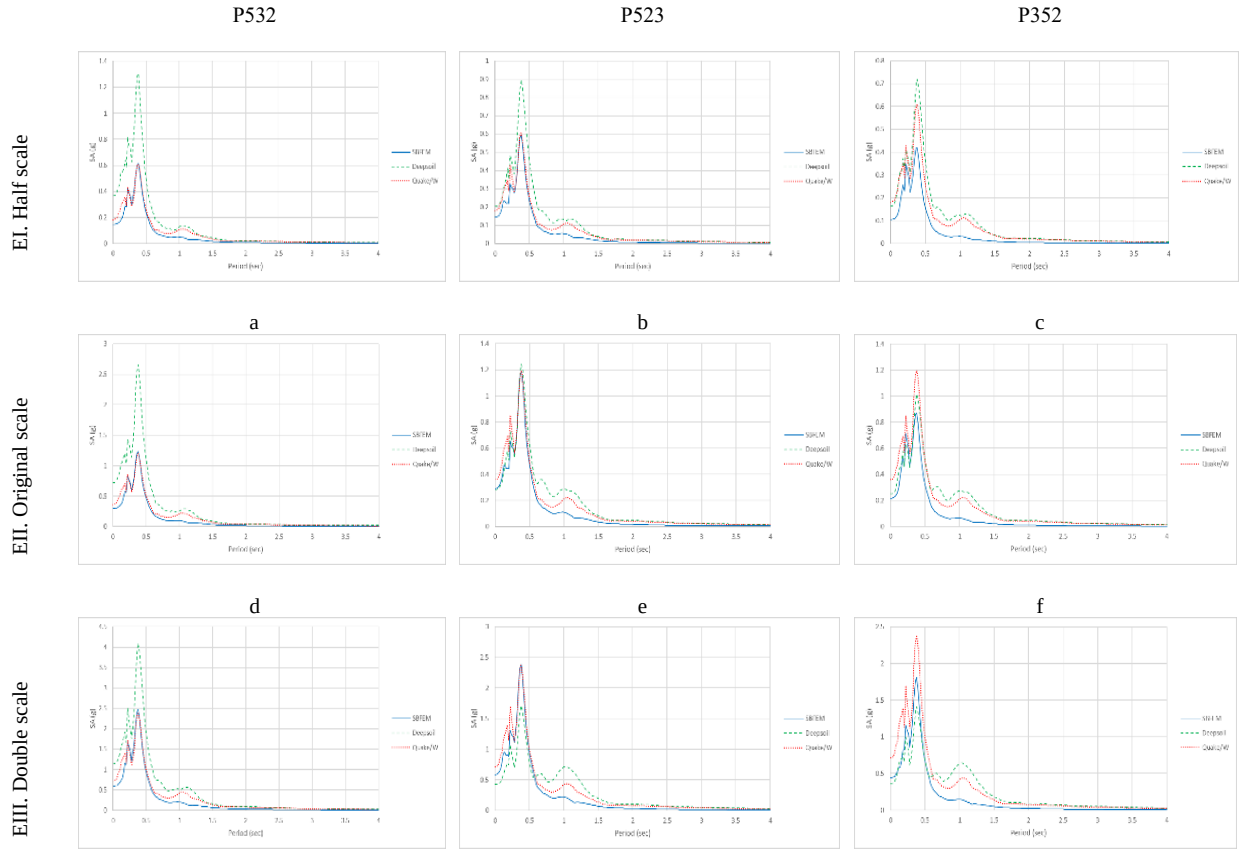


Figure 18. Acceleration response spectrum of Parkfield earthquakes for three layers soils

Table 7.

The peak percentage difference in the acceleration response spectrum of SBFEM compared to DEEPSOIL and QUAKE/W for Parkfield excitations of three-layer profiles

| | | Profile | | | | | |
|---|---|---|---|---|---|---|---|
| | | P532 | | P523 | | P352 | |
| | | DEEPSOIL | QUAKE/W | DEEPSOIL | QUAKE/W | DEEPSOIL | QUAKE/W |
| Excitation | EI | 53.0 | -0.5 | 33.9 | 2.1 | 41.6 | 31.1 |
| | EII | 53.6 | -2.5 | 4.5 | 0.6 | 14.4 | 27.5 |
| | EIII | 39.8 | -3.9 | -39.4 | -0.7 | -28.3 | 23.8 |

decreased depth. However, subtle deviations in deeper sublayers, particularly in P200 under excitations EI, EII, and EIII, suggest localized variations in soil behavior.

Similar to the single-layer cases, Fig. 19, as a sample, illustrates the final shear strain and shear modulus for the P532 profile under excitation EII. Across the three-layer profiles and intensity levels, shear strain consistently decreases with depth. In the P523 profile, a sharp strain drop occurs at the interface between 500 m $s^{-1}$ and 200 m $s^{-1}$ layers at 15 m depth, highlighting the strong influence of stiffness contrasts on strain distribution under dynamic loading.

### *4.3. Response Analysis of Nahanni Earthquake Simulations*

Using the same approach as for the Parkfield earthquake, the Nahanni earthquake was analyzed for single-layer profiles N200, N300, and N500 across three intensity levels.

Fig. 20, as the sample, shows the surface acceleration time history for N300 under excitation QII using SBFEM, compared with DEEPSOIL and QUAKE/W. DEEPSOIL consistently predicts higher accelerations for N200 and N300, particularly under excitations QI and QII. The peak acceleration response for the N200 profile under excitation Q1 are 39% and 55% lower for SBFEM and QUAKE/W respectively compared to DEEPSOIL, and for excitation Q2, these values are 25% and 38% lower, respectively.

Fig. 21 shows the acceleration response spectra for the Nahanni earthquake, highlighting the soil's frequency response. At lower periods, SBFEM and QUAKE/W results align closely, indicating similar accuracy. At longer periods, DEEPSOIL and QUAKE/W converge, suggesting shared modeling behavior. Table 8 lists the percentage differences in peak spectral values compared to DEEPSOIL and QUAKE/W for single-layer profiles.

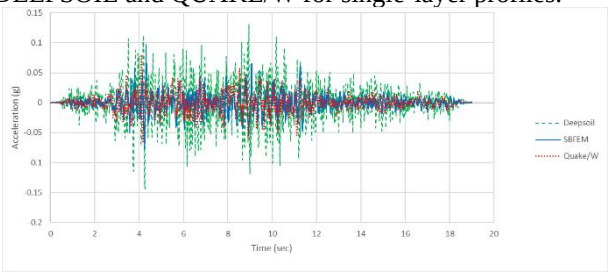


Figure 20. Response acceleration time history of profile N300 for excitation QII of Nahanni earthquake

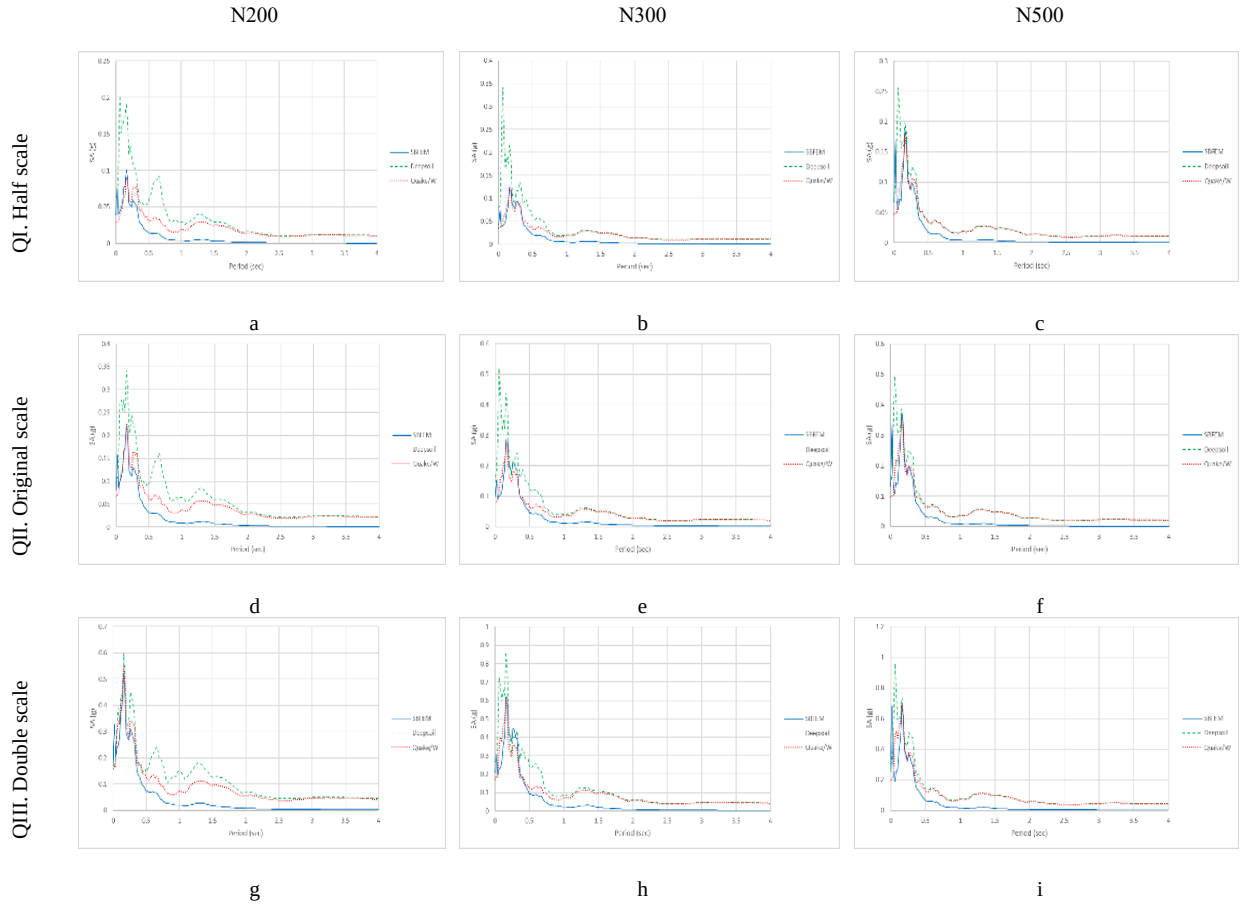


Figure 21. Acceleration response spectrum of Nahanni earthquakes for single layer soils

Table 8.
The peak percentage difference in the acceleration response spectrum of SBFEM compared to DEEPSOIL and QUAKE/W for Nahanni excitations of single layer profile

| | | Profile | | | | | |
|---|---|---|---|---|---|---|---|
| | | N200 | | N300 | | N500 | |
| | | DEEPSOIL | QUAKE/W | DEEPSOIL | QUAKE/W | DEEPSOIL | QUAKE/W |
| Excitation | QI | 47.5 | -12.0 | 42.7 | -0.9 | 6.7 | -4.7 |
| | QII | 35.2 | 2.2 | 34.5 | -2.0 | 3.2 | -6.1 |
| | QIII | 12.4 | 4.7 | 28.2 | -1.4 | 6.5 | 0.9 |

Fig. 22, an illustrative example, shows the final shear strain and shear modulus for N300 under excitation QII, highlighting earthquake-induced changes in mechanical properties. Shear strain increases with depth, while shear modulus generally rises toward the surface.

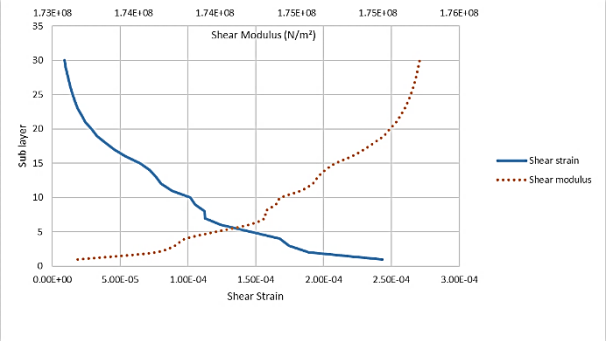


Figure 22. Shear strain and shear modulus of sublayers of profile N300 for excitation QII of Nahanni earthquake

The three-layer profiles N532, N523, and N352 were also analyzed under the same Nahanni earthquake intensity levels.

Fig. 23, as an example, shows the acceleration time history for N523 under excitation QII, and Fig. 24 presents surface response spectra for all three profiles. In the response acceleration time history for N532 and N352, DEEPSOIL and SBFEM results align closely, while QUAKE/W amplitudes are about 50% lower, suggesting similar sensitivity between DEEPSOIL and SBFEM. In contrast, for N523, SBFEM and QUAKE/W exhibit stronger agreement, with differences in response remaining below 10% for most of the analysis time steps, indicating their compatibility in modeling the unique characteristics of this profile.

In Fig. 24, DEEPSOIL consistently shows the highest spectral values—especially at natural periods—while SBFEM records the lowest, except in Fig. 24d. At higher periods, DEEPSOIL and QUAKE/W results overlap significantly, indicating similar performance in capturing long-period responses. Fig. 24d shows notable divergence, suggesting variability under certain seismic or soil conditions. Table 9 summarizes the percentage differences in peak spectral values between SBFEM, DEEPSOIL, and QUAKE/W for the three-layer profiles under the Nahanni earthquake.

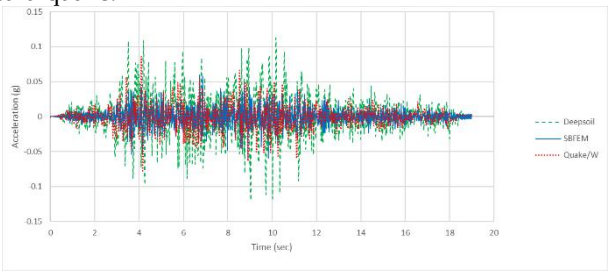


Figure 23. Response acceleration time history of profile N523 for excitation QII of Nahanni earthquake

As a sample, Fig. 25 presents the final shear strain and shear modulus for profile N523 under excitation QII. The results, which depict shear strain and shear modulus from the Nahanni earthquake show trends consistent with those observed in the Parkfield analyses.

## 5. Conclusions

This study has made a remarkably strong impact on the understanding of site response analysis in the geotechnical earthquake engineering discipline, combining versatile theoretical and computational techniques. Employing the SBFEM, we conducted a two-dimensional equivalent linear site response analysis that incorporated Rayleigh damping. Our results confirm that SBFEM provides a robust framework for accurately modeling the dynamic responses of soil layers to seismic activities. The method's ability to handle complex boundary conditions and its computational efficiency make it particularly suitable for analyzing earthquake-induced site responses.

We have successfully compared the SBFEM with traditional numerical methods, with the outcomes being similar and highly reliable, thus, clearly testifying to its precise performance in seismic analysis. The Rayleigh damping that is added to the SBFEM gives it an additional ability to simulate the real-world dissipation of energy by soils and thus, gives more information about the dampening characteristics during seismic events.

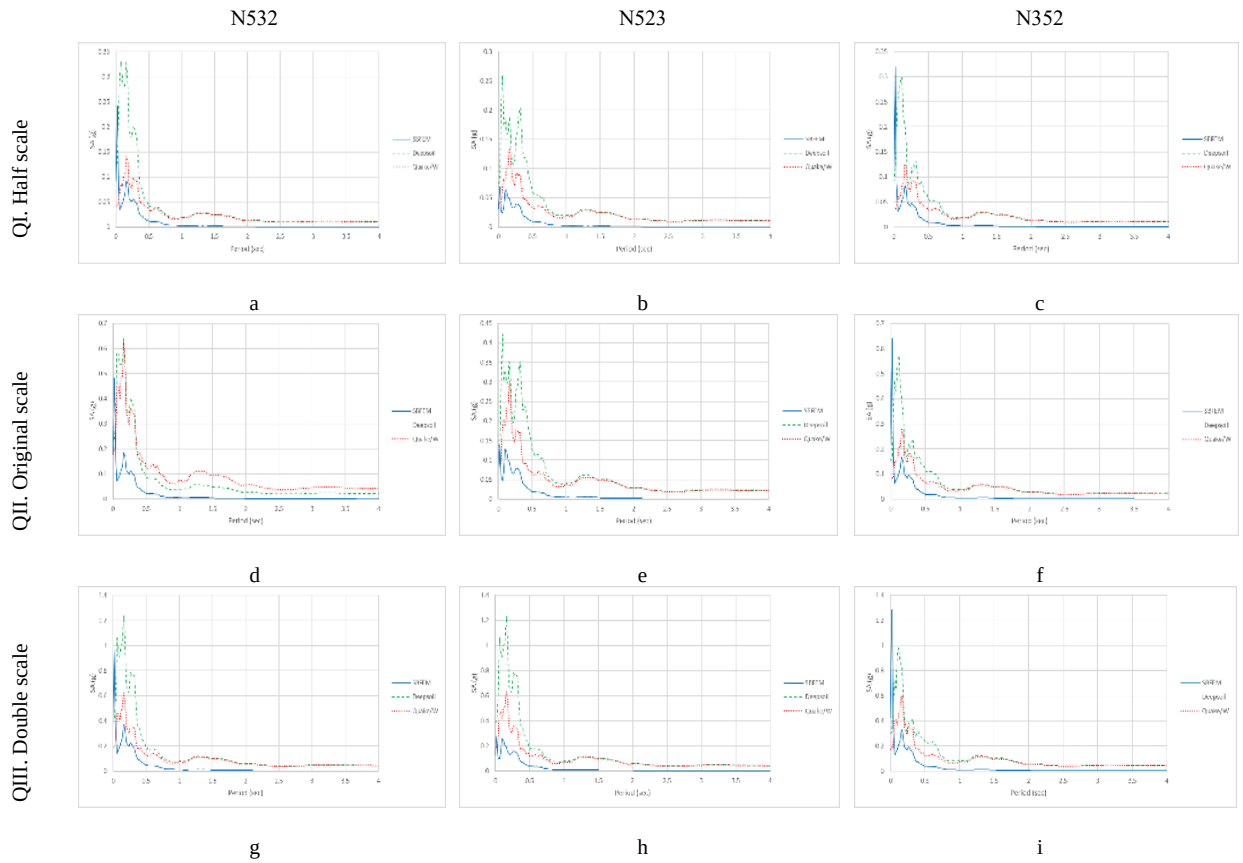


Figure 24. Acceleration response spectrum of Nahanni earthquakes for three layers soils

Table 9.

The peak percentage difference in the acceleration response spectrum of SBFEM compared to DEEPSOIL and QUAKE/W for Nahanni excitations of three-layer profiles

| | | **Profile** | | | | | |
|---|---|---|---|---|---|---|---|
| | | **N532** | | **N523** | | **N352** | |
| | | **DEEPSOIL** | **QUAKE/W** | **DEEPSOIL** | **QUAKE/W** | **DEEPSOIL** | **QUAKE/W** |
| **Excitation** | **QI** | 71.7 | 33.6 | 66.0 | 52.5 | 72.1 | 33.1 |
| | **QII** | 70.9 | 70.3 | 64.0 | 57.2 | 70.9 | 40.2 |
| | **QIII** | 69.8 | 40.6 | 79.1 | 59.6 | 66.1 | 44.5 |

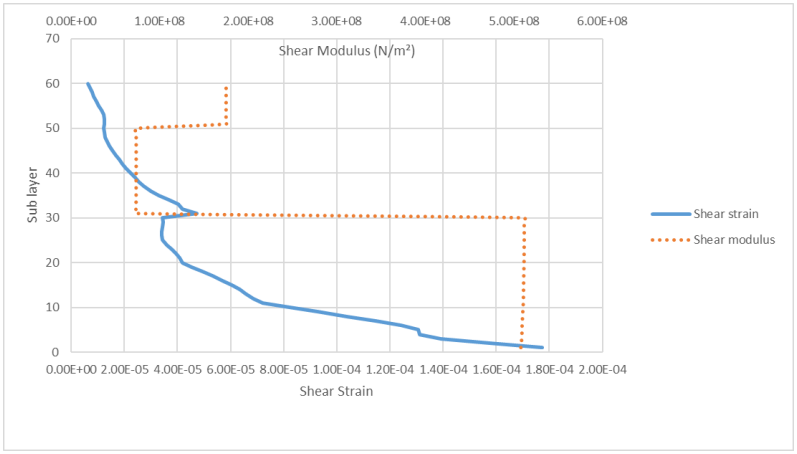


Figure 25. Shear strain and shear modulus of sublayers of profile N523 for excitation QII of Nahanni earthquake

Moreover, our research emphasizes the crucial influence of soil layer properties on seismic wave amplification and attenuation. Accurate characterization of these properties is essential for enhancing earthquake-resistant design and improving seismic risk assessments. The adaptation of SBFEM for various intensity excitations and for unbounded domains represents a significant methodological advancement, providing a powerful tool for more effectively predicting seismic responses. Besides, results highlight the importance of method choice in seismic analysis across varying soil types.

The implications of this research are significant for the field of geotechnical earthquake engineering, especially in regions susceptible to earthquakes. By delivering a more precise assessment of soil behavior under seismic loads, our approach can significantly contribute to the development of safer and more effective earthquake-resistant designs.

Future efforts will focus on the extension of SBFEM to non-linear site response analyses and the exploration of three-dimensional modeling capabilities. These advancements are expected to deepen our understanding of the complex interactions between soil layers and seismic waves, leading to enhanced predictive models and engineering solutions.

## References


[1] Jia, J. and Jia, J. "Site-response Analysis in Geotechnical Earthquake Engineering." Soil Dynamics and Foundation Modeling: Offshore and Earthquake Engineering (2018): 109–165. https://doi.org/10.1007/978-981-10-5773-9_4

[2] Boore, D. M. "Can Site Response Be Predicted?." Journal of Earthquake Engineering 8.spec01 (2004): 1–41. https://doi.org/10.1080/13632460409350519

[3] Wang, Z. and Carpenter, N. S. "Linear Site Responses from US Borehole Arrays: Primary Site-Response Parameters and Proxies." Soil Dynamics and Earthquake Engineering 164 (2023): 107578. https://doi.org/10.1016/j.soildyn.2022.107578

[4] Hashash, Y. M. A. et al. DEEPSOIL 7.0 User Manual. Urbana, IL: Board of Trustees of the University of Illinois at Urbana-Champaign, 2020.

[5] Kaklamanos, J., Baise, L. G., Thompson, E. M., and Dorfmann, L. "Comparison of 1D Linear, Equivalent-Linear, and Nonlinear Site Response Models at Six KiK-net Validation Sites." Soil Dynamics and Earthquake Engineering 69 (2015): 435–460. https://doi.org/10.1016/j.soildyn.2014.11.008

[6] Kim, B. et al. "Relative Differences Between Nonlinear and Equivalent-Linear 1D Site Response Analyses." Earthquake Spectra 32.3 (2016): 1845–1865. https://doi.org/10.1193/063015EQS107M

[7] Kramer, S. L. Geotechnical Earthquake Engineering. Upper Saddle River, NJ: Prentice Hall, 1996.

[8] Song, C. The Scaled Boundary Finite Element Method: Introduction to Theory and Implementation. Hoboken, NJ: John Wiley & Sons, 2018. https://doi.org/10.1002/9781119078388

[9] Semblat, J.-F. "Modeling Seismic Wave Propagation and Amplification in 1D/2D/3D Linear and Nonlinear Unbounded Media." International Journal of Geomechanics 11.6 (2011): 440–448. https://doi.org/10.1061/(ASCE)GM.1943-5622.0000050

[10] Bazyar, M. H. and Song, C. "Analysis of Transient Wave Scattering and Its Applications to Site Response Analysis Using the Scaled Boundary Finite-Element Method." Soil Dynamics and Earthquake Engineering 98 (2017): 191–205. https://doi.org/10.1016/j.soildyn.2017.04.013

[11] Tönük, G. and Ansal, A. "Factors Affecting Site-Specific Response Analysis." Journal of Earthquake Engineering 26.16 (2022): 8629–8646. https://doi.org/10.1080/13632469.2022.2085851

[12] Seed, H. B. Soil Moduli and Damping Factors for Dynamic Response Analyses, Report No. EERC-70. Berkeley, CA: Earthquake Engineering Research Center, University of California, 1970.

[13] Hashash, Y. M. A. and Park, D. "Non-Linear One-Dimensional Seismic Ground Motion Propagation in the Mississippi Embayment." Engineering Geology62.1–3 (2001): 185–206. https://doi.org/10.1016/S0013-7952(01)00047-0

[14] Park, D. and Hashash, Y. M. A. "Soil Damping Formulation in Nonlinear Time Domain Site Response Analysis." Journal of Earthquake Engineering 8.2 (2004): 249–274. https://doi.org/10.1080/13632460409350493

[15] Wolf, J. P. and Song, C. Finite-Element Modelling of Unbounded Media. Chichester: Wiley, 1996.

[16] Song, C. and Wolf, J. P. "The Scaled Boundary Finite-Element Method---Alias Consistent Infinitesimal Finite-Element Cell Method---for Elastodynamics." Computer Methods in Applied Mechanics and Engineering 147.3–4 (1997): 329–355. https://doi.org/10.1016/S0045-7825(97)00038-1

[17] Wolf, J. P. The Scaled Boundary Finite Element Method. Chichester: John Wiley & Sons, 2003.

[18] Khaji, N. and Khodakarami, M. I. "A New Semi-Analytical Method with Diagonal Coefficient Matrices for Potential Problems." Engineering Analysis with Boundary Elements 35.6 (2011): 845–854. https://doi.org/10.1016/j.enganabound.2010.12.006

[19] Zhang, X., Wegner, J. L., and Haddow, J. B. "Three-Dimensional Dynamic Soil-Structure Interaction Analysis in the Time Domain." Earthquake Engineering and Structural Dynamics 28.12 (1999): 1501–1524. https://doi.org/10.1002/(SICI)1096-9845(199912)28:12<1501::AID-EQE891>3.0.CO;2-Y

[20] Birk, C., Prempramote, S., and Song, C. "An Improved Continued-Fraction-Based High-Order Transmitting Boundary for Time-Domain Analyses in Unbounded Domains." International Journal for Numerical Methods in Engineering 89.3 (2012): 269–298. https://doi.org/10.1002/nme.3240

[21] Birk, C., Chen, D., Song, C., and Du, C. "The Scaled Boundary Finite Element Method for Transient Wave Propagation Problems." Seismic Design of Industrial Facilities: Proceedings of the International Conference on Seismic Design of Industrial Facilities (SeDIF-Conference) (2014): 547–556. https://doi.org/10.1007/978-3-658-02810-7_43

[22] Bazyar, M. H. and Song, C. "Transient Analysis of Wave Propagation in Non-Homogeneous Elastic Unbounded Domains by Using the Scaled Boundary Finite-Element Method." Earthquake Engineering & Structural Dynamics 35.14 (2006): 1787–1806. https://doi.org/10.1002/eqe.605

[23] Chen, X., Birk, C., and Song, C. "Transient Analysis of Wave Propagation in Layered Soil by Using the Scaled Boundary Finite Element Method." Computers and Geotechnics 63 (2015): 1–12. https://doi.org/10.1016/j.compgeo.2014.11.007

[24] Yaseri, A., Bazyar, M. H., and Hataf, N. "3D Coupled Scaled Boundary Finite-Element/Finite-Element Analysis of Ground

Vibrations Induced by Underground Train Movement." Computers and Geotechnics 60 (2014): 1–8. https://doi.org/10.1016/j.compgeo.2014.01.008

[25] Idriss, I. M. and Seed, H. B. Response of Horizontal Soil Layers During Earthquakes. Berkeley, CA: Earthquake Engineering Research Center, University of California, 1967.

[26] Schnabel, P. B. SHAKE: A Computer Program for Earthquake Response Analysis of Horizontally Layered Sites, Report No. EERC-72/12. Berkeley, CA: Earthquake Engineering Research Center, University of California, 1972.

[27] Idriss, I. M. and Sun, J. I. SHAKE91: A Computer Program for Conducting Equivalent Linear Seismic Response Analyses of Horizontally Layered Soil Deposits. Davis, CA: Center for Geotechnical Modeling, Department of Civil and Environmental Engineering, University of California, 1992.

[28] Ordonez, G. A. SHAKE2000: A Computer Program for the 1D Analysis of Geotechnical Earthquake Engineering Problems. Seattle, WA: GeoMotions, LLC, 2000.

[29] Vucetic, M. and Dobry, R. "Effect of Soil Plasticity on Cyclic Response." Journal of Geotechnical Engineering 117.1 (1991): 89–107. https://doi.org/10.1061/(ASCE)0733-9410(1991)117:1(89)

[30] Electric Power Research Institute (EPRI). Guidelines for Determining Design Basis Ground Motions, Final Report No. TR-102293. Palo Alto, CA: EPRI, 1993.

[31] Ishibashi, I. and Zhang, X. "Unified Dynamic Shear Moduli and Damping Ratios of Sand and Clay." Soils and Foundations 33.1 (1993): 182–191.

[32] Darendeli, M. B. Development of a New Family of Normalized Modulus Reduction and Material Damping Curves, PhD dissertation, University of Texas at Austin, 2001.

[33] Zhang, J., Andrus, R. D., and Juang, C. H. "Normalized Shear Modulus and Material Damping Ratio Relationships." Journal of Geotechnical and Geoenvironmental Engineering 131.4 (2005): 453–464. https://doi.org/10.1061/(ASCE)1090-0241(2005)131:4(453)

[34] Soliman, M. A. K. A. Dynamic Analysis of Unbounded Domain Problems by Applying the Scaled Boundary Finite-Element Method, MSc thesis, Faculty of Engineering Shoubra, Benha University, 2015.

[35] Khani, B. M. and Mohammad, H. Dynamic Soil-Structure Interaction Analysis Using the Scaled Boundary Finite-Element Method, PhD dissertation, UNSW Sydney, 2007.

[36] Radmanović, B. and Katz, C. "A High Performance Scaled Boundary Finite Element Method." IOP Conference Series: Materials Science and Engineering 10.1 (2010): 012214. https://doi.org/10.1088/1757-899X/10/1/012214

[37] Ju, S. H. and Ni, S. H. "Determining Rayleigh Damping Parameters of Soils for Finite Element Analysis." International Journal for Numerical and Analytical Methods in Geomechanics 31.10 (2007): 1239–1255. https://doi.org/10.1002/nag.586

[38] Bonet, J. and Wood, R. D. Nonlinear Continuum Mechanics for Finite Element Analysis. Cambridge: Cambridge University Press, 1997. https://doi.org/10.1017/CBO9780511755446

[39] Astley, R. J. Finite Elements in Solids and Structures: An Introduction. London: Chapman & Hall, 1992.